The role of intracellular pH in cell growth arrest induced by ATP

Sandrine Humez, Michaël Monet, Fabien van Coppenolle, Philippe Delcourt and Natalia Prevarskaya

Am J Physiol Cell Physiol 287:1733-1746, 2004. First published Sep 8, 2004;
doi:10.1152/ajpcell.00578.2003

Am J Physiol Cell Physiol 287: C1733–C1746, 2004.
First published September 8, 2004; doi:10.1152/ajpcell.00578.2003.

The role of intracellular pH in cell growth arrest induced by ATP

Sandrine Humez,[1,2] Michaël Monet,[1] Fabien van Coppenolle,[1] Philippe Delcourt,[1] and Natalia Prevarskaya[1]

[1]*Laboratoire de Physiologie Cellulaire, INSERM EMI 0228, Université des Sciences et Technologies de Lille, 59655 Villeneuve d'Ascq Cedex; and* [2]*Université d'Artois, Faculté Jean Perrin, 62300 Lens, France*

Submitted 23 December 2003; accepted in final form 23 August 2004

Humez, Sandrine, Michaël Monet, Fabien van Coppenolle, Philippe Delcourt, and Natalia Prevarskaya. The role of intracellular pH in cell growth arrest induced by ATP. *Am J Physiol Cell Physiol* 287: C1733–C1746, 2004. First published September 8, 2004; doi:10.1152/ajpcell.00578.2003.—In this study, we investigated ionic mechanisms involved in growth arrest induced by extracellular ATP in androgen-independent prostate cancer cells. Extracellular ATP reversibly induced a rapid and sustained intracellular pH (pH_i) decrease from 7.41 to 7.11. Inhibition of Ca^{2+} influx, lowering extracellular Ca^{2+}, and buffering cytoplasmic Ca^{2+} inhibited ATP-induced acidification, thereby demonstrating that acidification is a consequence of Ca^{2+} entry. We show that ATP induced reuptake of Ca^{2+} by the mitochondria and a transient depolarization of the inner mitochondrial membrane. ATP-induced acidification was reduced after the dissipation of the mitochondrial proton gradient by rotenone and carbonyl cyanide *p*-trifluoromethoxyphenylhydrazone, after inhibition of Ca^{2+} uptake into the mitochondria by ruthenium red, and after inhibition of the F_0F_1-ATPase with oligomycin. ATP-induced acidification was not induced by either stimulation of the Cl^-/HCO_3^- exchanger or inhibition of the Na^+/H^+ exchanger. In addition, intracellular acidification, induced by an ammonium prepulse method, reduced the amount of releasable Ca^{2+} from the endoplasmic reticulum, assessed by measuring change in cytosolic Ca^{2+} induced by thapsigargin or ATP in a Ca^{2+}-free medium. This latter finding reveals cross talk between pH_i and Ca^{2+} homeostasis in which the Ca^{2+}-induced intracellular acidification can in turn regulate the amount of Ca^{2+} that can be released from the endoplasmic reticulum. Furthermore, pH_i decrease was capable of reducing cell growth. Taken together, our results suggest that ATP-induced acidification in DU-145 cells results from specific effect of mitochondrial function and is one of the major mechanisms leading to growth arrest induced by ATP.

prostate; cancer; acidification

PROSTATE CANCER, ONE OF THE LEADING THREATS to men's health, progresses through an early stage that depends on androgens for growth and survival and during which androgen ablation therapy may cause tumors to regress; this stage is followed by the late, androgen-independent stage, for which there is currently no successful therapy (11). Indeed, little is known about the factors regulating the growth of androgen-independent prostate cancer cells. In this context, extracellular ATP is considered to be one of the physiological agents that inhibit the growth of several transformed cell lines through interactions with pharmacologically distinct P_2 purinergic receptors (12, 21). The concept that ATP may also function as a direct regulator of cell viability through the activation of P_2Y purinoreceptors in human androgen-dependent prostate carcinoma cell lines such as PC3, PC3-M, and DU-145 has been explored (10, 18). However, the ATP signal transduction mechanism inducing this important physiological effect on cell growth remains unknown. Recently, investigators at our laboratory (43) showed that ATP induces Ca^{2+} release from internal stores through the activation of the inositol 1,4,5-trisphophate (IP_3) type 3 receptor (IP_3R3) and the capacitative Ca^{2+} entry coupled to PLC activation. Furthermore, we suggest that growth arrest induced in DU-145 cells by extracellular ATP is correlated with a decrease in the intracellular Ca^{2+} concentration ($[Ca^{2+}]_i$). However, it is not clear whether this decrease in $[Ca^{2+}]_i$ directly induces the growth arrest in DU-145.

pH plays a central role in the regulation of many aspects of cell physiology, and protons may function as a second messenger in a manner similar to that of Ca^{2+} (3). Relatively small changes in pH_i could have a profound effect on a variety of cellular functions. For example, pH_i plays a role in the control of DNA synthesis, cellular proliferation, protein synthesis rate, cell fertilization, cell volume regulation, muscle contractility, neurotransmitter reuptake, and apoptosis. pH is also one of the factors thought to control the rate of cell proliferation and transformation (22, 37). It is now established that the pH_i of transformed cells is often more alkaline than that of normal cells (22, 32). In addition, because intracellular alkalinization has been shown to be involved in cell proliferation, a correlation between pH_i and cell cycle has been suggested (32). Thus a causative link between cellular pH homeostasis and tumor development has been suggested repeatedly, and elevated pH_i has been demonstrated to parallel both cell transformation and cell proliferation. Furthermore, Reschkin et al. (31) demonstrated that alkalinization is an early event in malignant transformation. In addition, the acid extrusion mechanism Na^+/H^+ exchanger (NHE) isoform 1 (NHE1) has been shown to play a key role in cell survival and proliferation (26), and NHE1 transcription is known to be strongly enhanced during cell proliferation (44). More recently, it was clearly shown that increased pH_i promotes the timing of the entry and transition of second growth phase and mitosis (G_2/M) (30). It is therefore possible to suggest that lowering pH_i may also reduce cell proliferation and/or induce apoptosis. To date, results concerning pH_i regulation and its involvement in prostate cancer cell physiology are lacking. Thus the main goal of this study was to evaluate the role of pH_i in the regulation of androgen-independent prostate cancer cell physiology. More particularly, this work focuses on the effect of external ATP on DU-145 cells because *1*) ATP regulates the growth of these cells and *2*) ATP

Address for reprint requests and other correspondence: S. Humez, Laboratoire de Physiologie Cellulaire, INSERM EMI 0228, Université des Sciences et Technologies de Lille, Bât. SN3, 59655 Villeneuve d'Ascq Cedex, France (E-mail: sandrine.humez@univ-lille1.fr).

The costs of publication of this article were defrayed in part by the payment of page charges. The article must therefore be hereby marked "*advertisement*" in accordance with 18 U.S.C. Section 1734 solely to indicate this fact.

has been shown to modulate pH_i in epithelial cells (19, 25, 28, 42) by mechanisms that are poorly understood.

It is now well established that cross talk exists between pH_i and intracellular Ca^{2+}. In effect, pH_i has been described as being able to affect intracellular Ca^{2+} homeostasis and contribute to the length, magnitude, and frequency of the Ca^{2+} signal through the modulation of voltage-dependent or -independent plasma membrane Ca^{2+} channels and/or through regulation of the mobilization of Ca^{2+} from internal stores (3, 7, 8, 16). On the other hand, Ca^{2+} has been described as inducing pH_i variation, particularly in neurons (1, 4, 36, 40, 47). In androgen-independent prostate cancer cells, external nucleotides induce a rapid intracellular Ca^{2+} increase (a few seconds after ATP application) and a long-term decrease in releasable Ca^{2+} from intracellular stores (after ATP has been applied for 2 days) (43). Thus the aim of the present study was to evaluate possible cross talk between the change in intracellular Ca^{2+} and pH_i and vice versa, as well as the possible implication of this cross talk in the growth regulation induced by ATP in androgen-independent prostate cancer cells.

The results of the present study show that ATP induces intracellular acidification of DU-145. This acidification is clearly linked to Ca^{2+} entry because of the ATP exposure of these cells. In addition, we show that acidification is linked to mitochondrial function and particularly to the F_0F_1-ATPase. We also demonstrate that ATP-induced acidification was not induced by stimulation of the Cl^-/HCO_3^- exchanger or by inhibition of NHE. Our finding leads us to suggest the existence of cross talk between pH_i and Ca^{2+} homeostasis in which the Ca^{2+}-induced intracellular acidification can in turn reduce the amount of releasable Ca^{2+} from the endoplasmic reticulum. We also suggest that ATP-induced acidification in DU-145 cells induced by the short-term Ca^{2+} response to ATP is one of the mechanisms leading to the long-term effect of ATP on Ca^{2+} homeostasis previously described in our model (43). Furthermore, we show that a decrease in pH_i, induced by 48-h dimethyl amiloride (DMA) treatment, was able to reduce cell growth. In conclusion, the present results suggest that acidification is one of the major mechanisms leading to growth arrest induced by ATP. Our results also highlight the physiological role of pH_i in the growth of prostate cancer cells and the cross talk between pH_i and Ca^{2+} response in these cells.

METHODS

Cell culture. The androgen-independent human prostate cancer cell line DU-145, obtained from the American Type Culture Collection (Manassas, VA), was maintained in culture in RPMI 1640 medium (Gibco/Life Technologies) supplemented with 10% fetal calf serum (Seromed; Poly-Labo, Strasbourg, France) and 5 mM L-glutamine (Sigma, L'Isle d'Abeau, France). Cells were grown at 37°C in a humidified atmosphere containing 5% CO_2. Before fluorescence measurements, the cells were trypsinized and transferred to glass coverslips. Cells were used 1–4 days after trypsinization. The medium was replaced every 24 h.

Ca^{2+} measurements using fura-2 AM. The culture medium was replaced by HBSS containing (in mM) 142 NaCl, 5.6 KCl, 1 $MgCl_2$, 2 $CaCl_2$, 0.34 Na_2HPO_4, 0.44 KH_2PO_4, 4.2 $NaHCO_3$, 10 HEPES, and 5.6 glucose. The osmolarity and pH of this solution were adjusted to 310 mosM and 7.4, respectively. When a Ca^{2+}-free medium was required, $CaCl_2$ was omitted and replaced by equimolar $MgCl_2$. Dye loading was achieved by transferring the cells into a standard HBSS solution containing 3 μM fura-2 acetoxymethyl ester (fura-2 AM; Calbiochem, Meudon, France) for 40 min at room temperature, then rinsing them three times with dye-free solution. Intracellular Ca^{2+} was measured using an imaging system (Princeton, Evry, France). The glass coverslip was mounted in a chamber on an Olympus microscope equipped for fluorescence. Fura-2 fluorescence was excited at 340 and 380 nm, and emitted fluorescence was measured at 510 nm (long-pass filter). The cytosolic Ca^{2+} concentration ($[Ca^{2+}]_i$) was derived from the ratio of the fluorescence intensities for each of the excitation wavelengths (F_{340}/F_{380}) and the Grynkiewicz equation. Ca^{2+} measurements using fura-2 AM were performed at 33°C. The cells were continuously perfused with HBSS solution, and chemicals were added via a whole chamber perfusion system. The flow rate of the whole chamber perfusion system was set at 1 ml/min, and the chamber volume was 500 μl.

Direct quantification of endoplasmic reticulum Ca^{2+} concentration. To obtain images of $[Ca^{2+}]$ within the endoplasmic reticulum ($[Ca^{2+}]_{ER}$), DU-145 cells were loaded with 2 μM Mag fura-2 (the AM derivative of Mag fura-2) for 45 min at 37°C. After incubation with the dye, the cells were rinsed briefly in a high-K^+ solution (in mM) composed of 125 KCl, 25 NaCl, 10 HEPES, and 0.1 $MgCl_2$, pH 7.2, and then exposed for 2 min to an intracellular buffer at 33°C and 5 μg/ml digitonin. Digitonin-permeabilized cells were continuously superfused with a digitonin-free intracellular buffer supplemented with 0.2 mM MgATP and free $[Ca^{2+}]$ clamped to 170 nM using a Ca^{2+}-ethylene glycol-bis(2-aminoethylether)-tetraacetic acid (EGTA) buffer. The Mag fura-2 fluorescence ratio was calibrated using exposure to 10 μM ionomycin and 15 mM Ca^{2+} or 10 mM EGTA, assuming a dissociation constant for Ca^{2+}-Mag fura-2 at room temperature of 53 μM. Ratio imaging measurements of Mag fura-2 fluorescence were obtained using an imaging system (Princeton).

pH_i measurements with BCECF. Dye loading was achieved by transferring the cells into a standard HBSS solution containing 1 μM 2′,7′-bis(carboxyethyl)-5(6)-carboxyfluorescein (BCECF)-AM for 20 min at room temperature, then rinsing the cells three times with dye-free solution. pH_i was measured using an imaging system (Princeton). The glass coverslip was mounted in a chamber on an Olympus microscope equipped for fluorescence. BCECF fluorescence was excited at 490 and 440 nm, and emitted fluorescence was measured at 530 nm (long-pass filter). The F_{490}/F_{440} emission ratio was converted to a linear pH scale using in situ calibration data obtained according to the nigericin technique. The cells were continuously perfused with HBSS, and chemicals were added via a whole chamber perfusion system. The flow rate of the whole chamber perfusion system was set at 1 ml/min, and the chamber volume was 500 μl. pH_i measurements with BCECF were performed at 33°C. In some experiments, extracellular Na^+ ions were replaced with *N*-methyl-D-glucamine, or Cl^- ions were replaced by methane sulfonate.

Mitochondrial $[Ca^{2+}]$ measurements. Fluorescence analysis was performed using a Zeiss LSM 510 confocal microscope (Carl Zeiss, Le Pecq, France) connected to a Zeiss Axiovert 200 M with a ×63 oil-immersion objective lens (numerical aperture 1.4). The image acquisition characteristics (e.g., pinhole aperture, laser intensity, scan speed) were the same throughout the experiments to ensure the comparability of the results. The confocal microscope software AIM 3.2 (Carl Zeiss) was used for data acquisition and analysis.

Changes in mitochondrial $[Ca^{2+}]$ were monitored with the membrane-permeable dihydrorhod-2 AM. Dihydrorhod-2 AM was formed by reacting 10 μl of 1 mg/ml $NaBH_4$ with 40 μl of 1 mM rhod-2 AM stock solution. Chemical reduction of rhod-2 AM with sodium borohydride before loading enhanced the mitochondrial localization of the indicator. Dye loading was achieved by transferring the cells into a standard HBSS solution containing 5 μM dihydrorhod-2 AM for 30 min at 37°C, followed by rinsing with dye-free solution for at least 3 h before the onset imaging. The dye was excited by a 543-nm laser line, and emission from the dye was collected through a long-pass filter of 560 nm. Stimulation-induced increases in dihydrorhod-2 fluorescence

were plotted as F/F_{rest}, where F is the measured fluorescence and F_{rest} is the resting (i.e., prestimulation) fluorescence.

Mitochondrial potential measurements. Changes in mitochondrial potential were monitored with 5,5′,6,6′-tetrachloro-1,1′,3,3′-tetraethylbenzimidazolycarbocyanine iodide (JC-1). Fluorescence analysis was performed using a Zeiss LSM 510 confocal microscope. JC-1 was first dissolved in DMSO (5 mg/ml). Dye loading was achieved by transferring the cells into a standard HBSS solution containing 5 μg/ml of JC-1 for 20 min at 37°C. After the loading period, the cells were rinsed three times with dye-free solution. At high mitochondrial membrane potentials, JC-1 accumulates sufficiently in the mitochondria to form aggregates (J aggregates) that fluoresce red. At lower mitochondrial potentials, less dye enters the mitochondria, resulting in monomers that fluoresce green. Cells were excited by a 488-nm laser line, and fluorescence emission was recorded at 530 and 590 nm. Mitochondrial potential was expressed as the red-green fluorescence ratio.

Measurements of in vitro cell growth. Cells were seeded at an initial density of 900 cells/well in 96-well plates (Poly Labo, Strasbourg, France). After 48 h, cells were cultured in treatment medium (*day 0*). From *day 0*, the treatment medium was changed daily for each condition. Cells were harvested on *day 2*, and the cell number was determined using a colorimetric method. The CellTiter 96 aqueous nonradioactive cell proliferation assay (Promega, Madison, WI) was used to determine the number of viable cells. This commercial assay is composed of 3-(4,5-dimethylthiazol-2-yl)-5-(3-carboxymethoxyphenyl)-2-(4-sulfophenyl)-2H-tetrazolium salt (MTS) and phenazine methosulfate (PMS), an electron coupling reagent. MTS is bioreduced by cells into a formazan that is soluble in the cell culture medium. The absorbance of formazan at 490 nm is measured directly from 96-well assay plates. The formazan produced, measured by the amount of 490-nm absorbance, is directly proportional to the number of living cells in the culture. Dunnett's test was used for statistical analysis.

Data analysis. Statistical data refer to fluorimetric measurements of Ca^{2+} and pH in single cells from each coverslip. Data were normalized for presentation of some results, and values are relative to basal pH_i or $[Ca^{2+}]_i$, designated as 1. DMA (50 μM), 4,4′-diisothiocyanostilbene sulfonic acid (DIDS; 100 μM), and carbonyl cyanide *p*-trifluoromethoxyphenylhydrazone (FCCP; 5 μM) induced a reduction of the resting pH_i by ~0.2 pH unit. Oligomycin (2 μM) induced a reduction of the resting pH_i by ~0.1 pH unit. Results are expressed as means ± SD, where *n* indicates the number of cells used to express the mean. Plots were produced using Origin 5.0 software (Microcal Software); graphs are expressed as means ± SE. Each experiment was repeated several times. The Tukey-Kramer test was used for statistical comparison among means and differences, and $P < 0.05$ was considered significant.

Chemicals. Rotenone, nigericin, FCCP, 2-aminophenyl borate (2-APB), oligomycin, thapsigargin (TG), DIDS, DMA, ATP, EGTA-AM, ruthenium red, ionomycin, fura-2 AM, and BCECF-AM were purchased from Sigma. JC-1 and rhod-2 AM were obtained from Interchim.

RESULTS

Effect of ATP on pH_i and the involvement of PLC. Under control conditions, pH_i measured in DU-145 cells was 7.41 ± 0.18 ($n = 208$). A typical effect of extracellular ATP (100 μM) on pH_i in DU-145 cells is illustrated in Fig. 1*A*. In the presence of external Ca^{2+} (2 mM) exposure of DU-145 cells to ATP (100 μM) produced a rapid decrease of 0.31 ± 0.09 pH units ($n = 163$). This effect was reversible: removal of ATP from the bath solution was followed by pH_i recovery toward basal levels (Fig. 1*B*).

The activation of P_2X receptor in DU-145 cells was reported previously (18). Figure 1*C* shows that intracellular acidification induced by ATP is not linked to the activation of P_2X receptors, because inhibition of these P_2X receptors by 30 μM pyridoxal-phosphate-6-azophenyl-2′,4′-disulfonate (PPADS) did not affect the ATP response. It also was previously shown

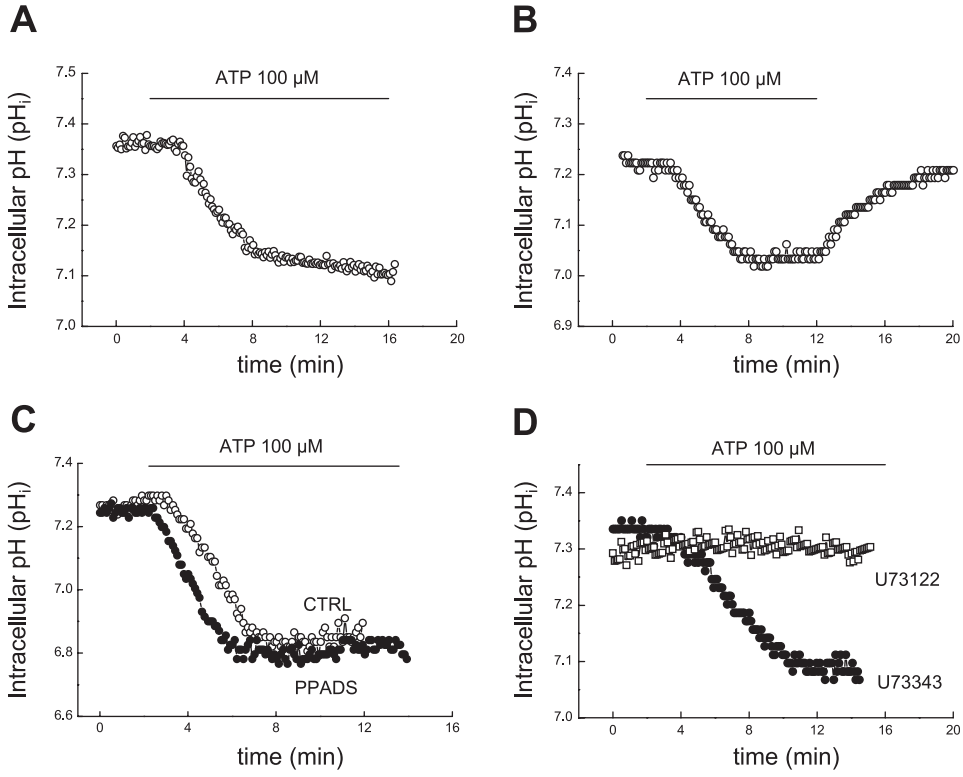

Fig. 1. ATP induces acidification linked to activation of PLC by the P_2 purinergic receptor. *A*: time course of change in intracellular pH (pH_i) after the application of 100 μM ATP to the extracellular medium. *B*: time course of change in pH_i after a transient application of 100 μM ATP to the extracellular medium. *C*: time course of changes in pH_i after application of 100 μM ATP to the extracellular medium ($n = 30$) or in the presence of 30 μM pyridoxal-phosphate-6-azophenyl-2′,4′-disulfonate (PPADS; $n = 56$). *D*: time course of change in pH_i after application of 100 μM ATP to the extracellular medium in the presence of 20 μM U-73122 (a PLC inhibitor; $n = 38$) or in the presence of 20 μM U-73343 (inactive analog of U-73122, $n = 36$). These results are representative of the mean.

that DU-145 express P_2Y receptors coupled to PLC (10). To determine PLC involvement in ATP-induced acidification, we inhibited the PLC pathway by preincubating cells for 45 min with U-73122 (20 μM), a PLC inhibitor, before applying ATP. U-73122 abolished the pH_i decrease ($n = 36$; Fig. 1*D*), whereas the same concentration of the inactive analog, U-73343, did not alter the ATP-induced intracellular acidification ($n = 38$; Fig. 1*D*).

Role of cytoplasmic Ca^{2+} increase in ATP-induced acidification. In DU-145 cells, external ATP is known to produce a large $[Ca^{2+}]_i$ increase (18, 43). We therefore investigated the role of Ca^{2+} in the ATP-induced acidification. Figure 2*A* clearly shows that 100 μM 2-APB, which blocks the ATP-induced Ca^{2+} entry in DU-145 (43), inhibits the effect of ATP on pH_i. In addition, incubation of DU-145 cells with the permeable Ca^{2+} chelator EGTA-AM (50 μM) also greatly reduced ATP-induced acidification (Fig. 2*B*). In effect, ATP induced a decrease of 0.33 ± 0.03 pH units ($n = 24$) in control conditions, whereas it induced decreases of 0.04 ± 0.01 ($n = 26$) and 0.05 ± 0.01 ($n = 30$) pH units when cells were treated with 100 μM 2-APB and 50 μM EGTA-AM, respectively (Fig. 2*C*). When applied to a Ca^{2+}-free medium, ATP induced only slight acidification (0.09 ± 0.02 pH units; $n = 25$) that greatly increased (to 0.29 ± 0.056 pH units; $n = 25$) when Ca^{2+} was readmitted to the bathing medium (Fig. 2*D*).

To further confirm the role of Ca^{2+} in ATP-induced acidification, we then tested the hypothesis that TG (1 μM), a sarcoplasmic Ca^{2+}-ATPase inhibitor that induces intracellular Ca^{2+} release from endoplasmic reticulum stores followed by the well-described capacitive Ca^{2+} entry, could mimic the acidification induced by ATP. We also investigated whether Ca^{2+}-induced intracellular acidification could be produced by the $[Ca^{2+}]_i$ increase induced by Ca^{2+} release and/or by Ca^{2+} influx. As shown in Fig. 3*A*, TG (1 μM) application to cells bathed in a Ca^{2+}-free medium were unable to induce intracellular acidification, whereas Ca^{2+} readmission to the bathing medium induced sustainable intracellular acidification. Furthermore, ionomycin (1 μM), which is widely used to increase intracellular Ca^{2+}, was also unable to induce intracellular acidification in a Ca^{2+}-free medium, whereas Ca^{2+} readmission to the bathing medium induced sustainable intracellular acidification (Fig. 3*B*). The magnitude of the intracellular acidification induced by TG and ionomycin was of the same order as that induced by ATP (Fig. 3*C*). Moreover, the addition of ATP after TG pretreatment failed to induce an additional and significant pH_i acidification (Fig. 3*D*). Taken together, these results clearly show that Ca^{2+} influx is involved in ATP-induced acidification.

Involvement of mitochondrial F_0F_1-ATPase in ATP-induced pH_i drop. Mitochondria are known to reuptake Ca^{2+} ions released into the cytoplasm during agonist stimulation, a process dependent on the membrane potential across the inner membrane (27, 34). In effect, when $[Ca^{2+}]_i$ reaches the level at which the rate of Ca^{2+} influx into the mitochondria exceeds the rate of Ca^{2+} extrusion from the mitochondria, the mitochondria start to accumulate Ca^{2+}, which depolarizes the inner mitochondrial membrane. To compensate for the mitochondrial membrane potential drop, regulatory mechanisms that extrude extra protons from the mitochondrial matrix are activated. For example, protons may be extruded by the mitochondrial F_0F_1-ATPase at the expense of cytoplasmic ATP (6). Recognizing that F_0F_1-ATPase can operate bidirectionally (2, 24), we investigated whether this ATPase could be responsible for the change in cytoplasmic pH induced by ATP.

To assess the role of mitochondria in ATP-induced acidification, we looked into whether ATP stimulation was able to induce Ca^{2+} influx into mitochondria and depolarization of the inner mitochondrial potential. To determine directly whether mitochondria take up Ca^{2+} after ATP stimulation, we imaged mitochondria using confocal microscopy and the mitochondrial Ca^{2+}-sensitive dye dihydro-rhod2. Dihydro-rhod2 imaging of DU-145 cells showed patchy staining in the cytosol, a

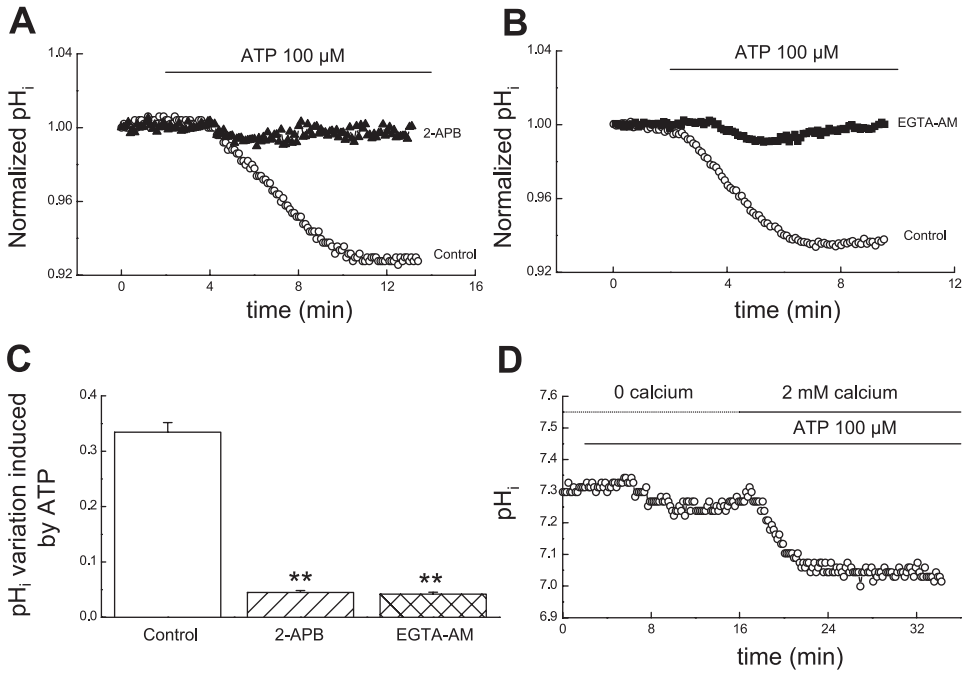

Fig. 2. ATP-induced acidification is a result of Ca^{2+} entry. *A*: typical traces showing the time course of change in pH_i after application of 100 μM ATP in the absence (control) or presence of 100 μM 2-aminophenyl borate (2-APB). Values are relative to basal pH_i, designated as 1. *B*: typical traces showing the time course of change in pH_i after application of 100 μM ATP in the absence (control) or presence of 50 μM ethylene glycol-bis(2-aminoethylether)-tetraacetic acid (EGTA-AM). Values are relative to basal pH_i, designated as 1. *C*: amplitude of the effect of 100 μM ATP (mean ± SE) under various conditions. Bars represent mean values of change in pH_i induced by ATP alone ($n = 24$) or in the presence of 2-APB ($n = 26$) and EGTA-AM ($n = 30$). $^{**}P < 0.01$, significantly different from control. *D*: typical traces of the time course of change in pH_i observed in a Ca^{2+}-free medium and in the presence of Ca^{2+} after 100 μM ATP application.

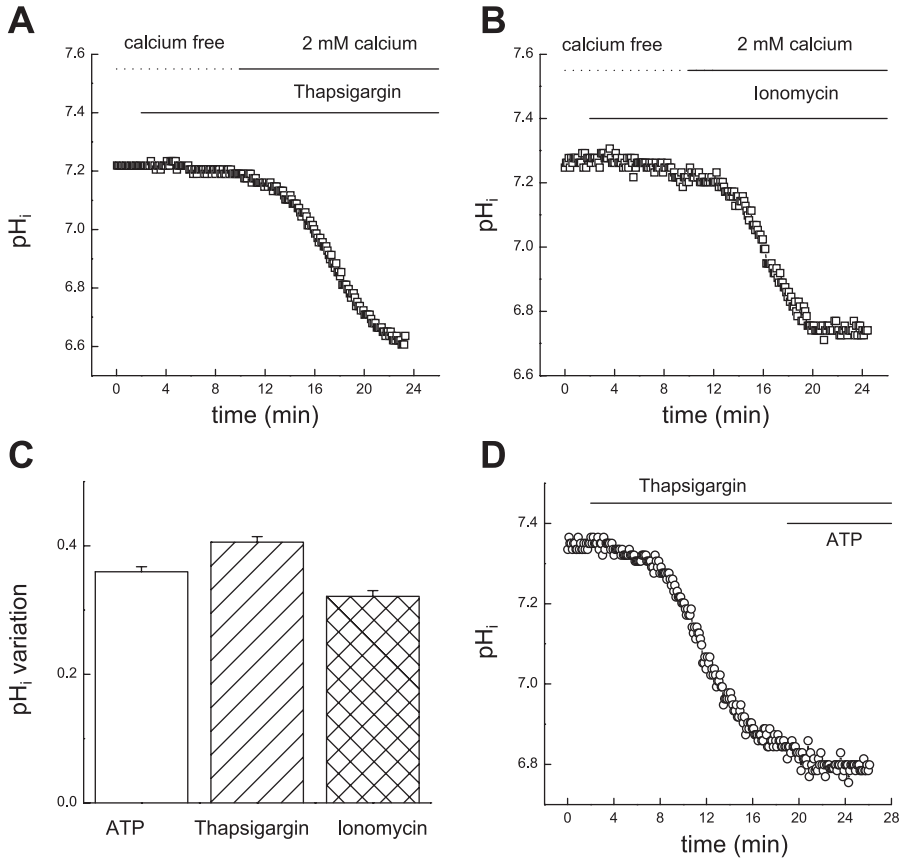

Fig. 3. Increase in the intracellular Ca^{2+} concentration ($[Ca^{2+}]_i$) induced by thapsigargin (TG) or ionomycin induced intracellular acidification. *A*: typical traces of the time course of change in pH_i observed in a Ca^{2+}-free medium and in the presence of Ca^{2+} after 1 μM TG application. *B*: typical traces of the time course of change in pH_i observed in a Ca^{2+}-free medium and in the presence of Ca^{2+} after 1 μM ionomycin application. *C*: amplitude of the acidification induced by 100 μM ATP ($n = 24$), 1 μM TG ($n = 28$), and 1 μM ionomycin ($n = 33$). The magnitude of the ATP-induced acidification in this experiment was 0.35 ± 0.06 pH units ($n = 24$), and those induced by TG and ionomycin were 0.40 ± 0.07 pH units ($n = 28$) and 0.32 ± 0.09 pH units ($n = 33$), respectively. Bars represent change in pH_i expressed as means ± SE. *D*: typical trace showing the time course of change in pH_i after 1 μM TG exposure and subsequent extracellular 100 μM ATP application. These results are representative of the mean values.

pattern compatible with preferential staining of mitochondria using dihydro-rhod2 (Fig. 4*A*).The application of 100 μM ATP resulted in a large increase in fluorescence ($F/F_{rest} = 1.46 \pm 0.22$; $n = 15$), suggesting that mitochondria take up Ca^{2+} after ATP stimulation (Fig. 4*B*). Changes in mitochondrial potential were investigated using confocal microscopy and the mitochondria-specific, voltage-sensitive dye JC-1. Unstimulated cells displayed patchy red fluorescence, which indicates a polarized state (Fig. 4*Ca*). As shown in Fig. 4*Cb*, the addition of ATP induced dissipation of the mitochondrial potential. FCCP (5 μM) cause the mitochondrial potential to collapse dramatically and served as a positive control (Fig. 4*Cc*). The variation in the mitochondrial potential was plotted as the red-green fluorescence ratio. When cells were perfused with 100 μM ATP, the depolarization of the mitochondria was observed and identified as a decrease in the JC-1 fluorescence ratio (Fig. 4*D*). ATP-evoked depolarization of mitochondria was transient ($n = 41$), indicating a regulation of the mitochondrial potential.

We therefore reduced the proton gradient across the inner mitochondrial membrane with 10 μM rotenone, a mitochondrial toxin that is a potent and competitive inhibitor of the complex I respiratory chain. Treating DU-145 cells with 10 μM rotenone for up to 30 min decreased the ATP-induced acidification (Fig. 5*A*). As shown in Fig. 5*B*, in the presence of rotenone, the ATP-induced acidification was 0.07 ± 0.07 pH units ($n = 55$), corresponding to 41% of the pH_i variation induced by ATP under control conditions (0.17 ± 0.04 pH units; $n = 47$). As shown in Fig. 5, *C* and *D*, rotenone was unable to modify the amount of $[Ca^{2+}]_i$ increase induced by ATP in our experimental conditions. Indeed, the $[Ca^{2+}]_i$ increase induced by ATP was 786 ± 268 nM ($n = 45$) in control conditions, whereas it was 756 ± 190 nM ($n = 53$) when cells were treated for 30 min with 10 μM rotenone. This result suggests that rotenone does not act on pH_i by altering the Ca^{2+} response to ATP.

We then used a protonophore (H^+ ionophore) to collapse the mitochondrial membrane potential. FCCP uncouples mitochondrial respiration and ATP production by dissipating the proton gradient across the inner mitochondrial membrane, and it is also known to prevent mitochondrial Ca^{2+} uptake (13, 14, 32). Cells were treated for 30 min with 5 μM FCCP, and then ATP (100 μM) was applied. This treatment reduced the ATP-induced acidification by 48% (Fig. 6*A*). Indeed, the magnitude of the ATP-induced acidification in control conditions was 0.29 ± 0.06 pH units ($n = 64$), whereas it was 0.15 ± 0.06 pH units ($n = 62$) when cells were treated with FCCP (Fig. 6*D*). FCCP-treated cells exhibit a smaller $[Ca^{2+}]_i$ increase when challenged by 100 μM ATP compared with cells treated with ATP alone (Fig. 6*G*). The variation of $[Ca^{2+}]_i$ induced by ATP was 786 ± 268 nM ($n = 49$) under control conditions, compared with 627 ± 103 nM ($n = 30$) when cells were treated with 5 μM FCCP.

Oligomycin is a selective inhibitor of membrane-bound mitochondrial F_0F_1-ATPase. In the presence of oligomycin, both synthesis and hydrolysis of ATP by the mitochondria, as well as proton movement, are prevented (24). The incubation of DU-145 cells with 2 μM oligomycin reduced the magnitude of ATP-induced acidification (Fig. 6*B*). In the presence of oligomycin, ATP-induced acidification was 0.11 ± 0.05 pH

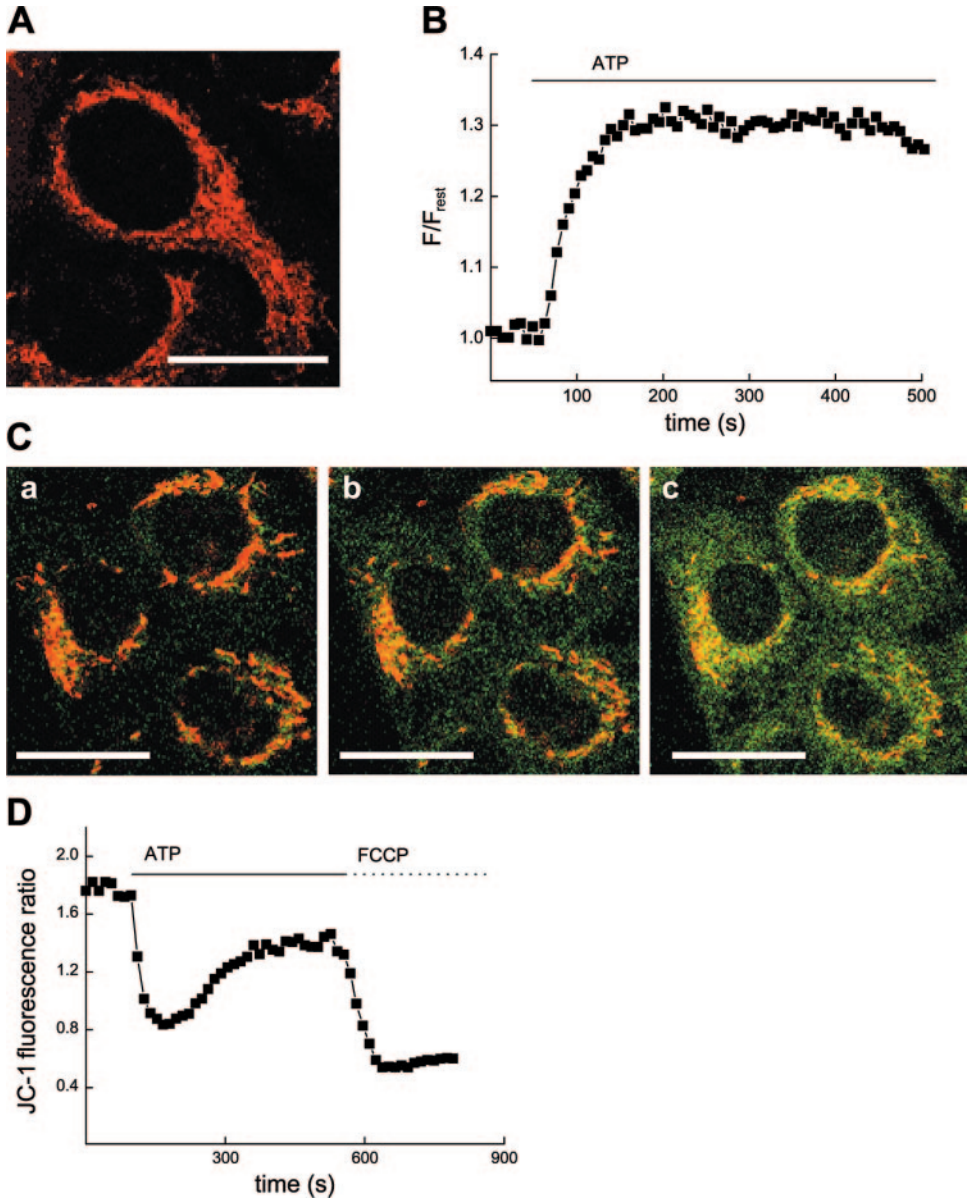

Fig. 4. ATP increases mitochondrial [Ca^{2+}] and decreases the mitochondrial potential. *A*: confocal microscopic image showing a DU-145 cell loaded with dihydro-rhod2. The rhod-2 fluorescence is localized in mitochondria. *B*: time course of ATP-induced increase in mitochondrial [Ca^{2+}]. *C*: confocal microscopic images showing a DU-145 cells loaded with 5,5′,6,6′-tetrachloro-1,1′,3,3′-tetraethylbenzimidazolycarbocyanine iodide (JC-1) before ATP stimulation (*a*), during ATP (100 μM) stimulation (*b*), and during carbonyl cyanide *p*-trifluoromethoxyphenylhydrazone (FCCP; 5 μM) application (*c*). *D*: time course of ATP induced a transient loss of mitochondrial potential and subsequent effect of FCCP. Stimulation of DU-145 cells led to a decrease in fluorescence of JC-1 ratio, as an index of mitochondrial depolarization. Bars, 20 μM.

units ($n = 61$), corresponding to 39% of the control conditions (0.28 ± 0.05 pH units; $n = 60$). Oligomycin (2 μM) was unable to significantly modify the amplitude of the ATP-induced increase in [Ca^{2+}]$_i$ (Fig. 6*G*). In the presence of oligomycin, the amplitude of the [Ca^{2+}]$_i$ increase induced by ATP (100 μM) was 730 ± 200 nM ($n = 40$), whereas it was 786 ± 268 nM ($n = 49$) when cells were kept under control conditions. Furthermore, specific inhibition of the vacuolar type H^+-ATPase with bafilomycin had no effect on cytoplasmic acidification induced by ATP (data not shown).

Inhibition of the mitochondrial Ca^{2+} uniporter with ruthenium red also reduced ATP-induced acidification. Treating DU-145 cells with 30 μM ruthenium red for 30 min decreased ATP-induced acidification by 67% (Fig. 6*C*). In the presence of ruthenium red, ATP-induced acidification was 0.10 ± 0.01 pH units ($n = 45$), whereas it was 0.32 ± 0.02 pH units ($n = 44$) for untreated cells (Fig. 6*F*). As shown in Fig. 6*G*, ruthenium red was unable to modify the amount of [Ca^{2+}]$_i$ increase induced by ATP in our experimental conditions.

Taken together, these data indicate that a specific effect on the mitochondrial function accounts for ATP-induced acidification in DU-145 cells. We therefore conclude that F_0F_1-ATPase may participate in pH_i acidification induced by ATP.

Cl^-/HCO_3^- exchanger and NHE involvement in ATP-induced acidification. We also tested the possibility of the involvement of the Cl^-/HCO_3^- exchanger in the extracellular ATP effect, because its binding to a P_2 purinergic receptor leads, in some models, to an enhancement of the Cl^-/HCO_3^- exchanger (49). The presence of the Cl^-/HCO_3^- exchanger was studied by measuring the change in pH_i induced by a Cl^--free medium. Changing the extracellular medium from the control medium to the Cl^--free medium produced a pronounced increase in pH_i (mean range, 0.58 ± 0.17 pH units; $n = 72$). No change in pH_i was observed when the Cl^--free medium was applied in the presence of 100 μM DIDS, a Cl^-/HCO_3^- exchanger inhibitor (Fig. 7*A*). To investigate the involvement of exchange in the ATP effect, we measured the change in pH_i induced by ATP in Cl^--free medium and in the presence of

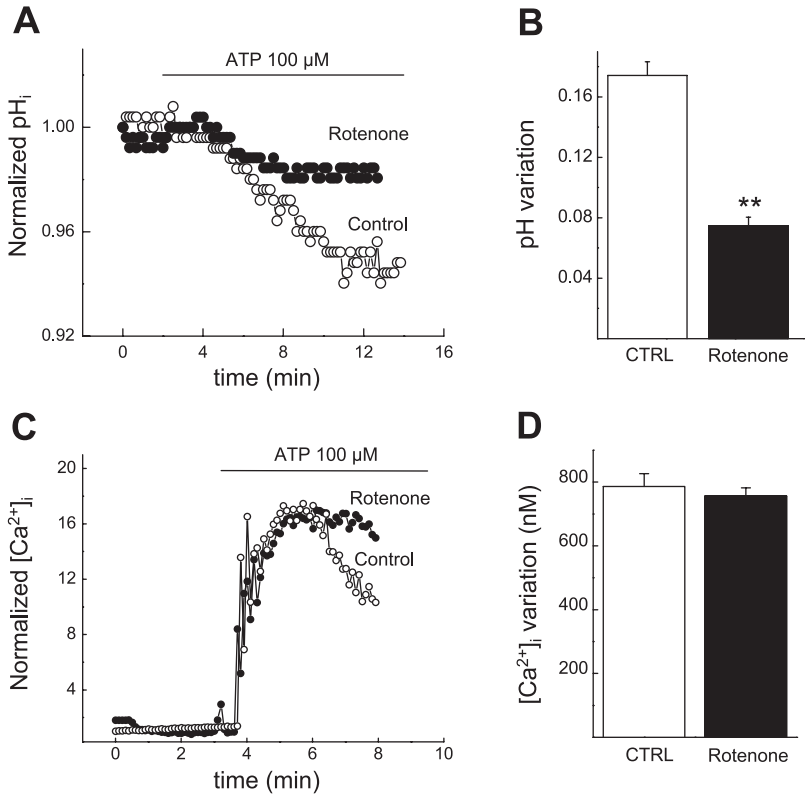

Fig. 5. Rotenone decreases ATP-induced intracellular acidification without affecting the amplitude of the increased $[Ca^{2+}]_i$. *A*: typical traces showing the time course of change in pH_i after an application of 100 μM ATP in the absence (control, open circles) or in the presence of 10 μM rotenone (rotenone, closed circles). Values are relative to basal pH_i, designated as 1. *B*: mean value of change in pH_i induced by 100 μM ATP under control conditions (CTRL; $n = 47$) and in the presence of 10 μM rotenone ($n = 55$). $^{**}P < 0.01$, significantly different from control. Bars represent change in pH_i and are expressed as means ± SE. *C*: typical traces showing the time course of changes in $[Ca^{2+}]_i$ after application of 100 μM ATP in the absence (control, open circles) or in the presence of 10 μM rotenone (closed circles). Values are relative to basal $[Ca^{2+}]_i$, designated as 1. *D*: mean value of changes in the $[Ca^{2+}]_i$ induced by 100 μM ATP under control conditions (CTRL; $n = 45$) and in the presence of 10 μM rotenone ($n = 53$). Bars represent change in the $[Ca^{2+}]_i$ and are expressed as means ± SE.

DIDS. Figure 7*B* illustrates that the effect of ATP on pH_i was not inhibited in the Cl^--free medium, with all cells showing a pH_i decrease of ~0.25 ± 0.10 pH units ($n = 14$). As shown in Fig. 7*C*, the effect of ATP on pH_i was not inhibited by DIDS. Indeed, ATP-induced acidification was identical to the control conditions when cells were treated with 100 μM DIDS (100 ± 17%; $n = 23$). These latter results suggest that ATP-induced acidification is not mediated by activation of the Cl^-/HCO_3^- exchanger. In contrast, the activity of the Cl^-/HCO_3^- exchanger was reduced when ATP was applied to DU-145 cells, because the pH_i variation induced by the Cl^--free medium was smaller when ATP was present in the bathing solution (Fig. 7, *D–F*). Indeed, pH_i increase induced by the Cl^--free medium was 0.58 ± 0.17 pH units ($n = 72$) in control condition, while it was 0.41 ± 0.12 pH units ($n = 51$) for 100 μM ATP-treated cells.

We then tested whether NHE could be involved in the ATP-induced pH_i decrease, because it has been described that NHE can be involved in ATP-induced intracellular acidification (42). Figure 8*A* shows that extracellular NH_4^+ caused pH_i to rise. This alkalinization is thought to result from the rapid influx of NH_3 and the subsequent combination of these molecules with intracellular H^+ (35). This was followed by a slow fall in pH_i caused by the entry of NH_4^+ and its dissociation into NH_3 and H^+. The subsequent removal of extracellular NH_4^+ causes a fall in pH_i due to the dissociation of NH_4^+ into H^+, which remains in the cells, and NH_3, which can leave the cytoplasm. This causes an underestimate of the pH_i below the starting value. pH_i subsequently recovered as a result of the activity of acid-extruding systems present in the cells. Recovery was extremely sensitive to 50 μM DMA, an inhibitor of NHE. This inhibitory effect of DMA was reversible (Fig. 8*B*). These results lead us to conclude that an amiloride-sensitive NHE is responsible for recovery from an induced acid load under our experimental conditions. Blocking NHE with DMA (50 μM) did not prevent ATP-induced acidification (Fig. 8*C*, $n = 13$). This result suggests that ATP-induced acidification is not the result of an inhibition of NHE.

Physiological significance of ATP-induced acidification. It is now well established that ATP reduces the growth of DU-145 cells (18, 43). This reduction in cell growth is concomitant with a decrease in the amount of releasable Ca^{2+} shown to be able to mediate growth arrest (43). Figure 9 shows that ATP-induced reduction of cell growth (Fig. 9*A*) correlates with the amplitude of the Ca^{2+} increase (Fig. 9*B*) and with a decrease in pH_i (Fig. 9*C*) in a dose-dependent manner. The growth rate inhibition induced by ATP cannot be explained by an increase in apoptosis, because no stimulation of apoptosis was observed in our experiments as determined with Hoechst staining (data not shown).

Because it has been demonstrated that ATP induced a reduction in the releasable Ca^{2+} involved in the decrease in cell growth, we postulated that the decrease in the pH_i induced by ATP could be a part of the mechanism that leads to the reduction in releasable Ca^{2+}. Therefore, we tested the effect of artificial acidification induced by an NH_4^+ pulse in the presence of DMA on the ability of TG and ATP to release intracellular Ca^{2+} in DU-145 cells. As shown in Fig. 9*D*, *inset*, when cells were submitted to an NH_4^+ pulse (20 mM) for 5 min in a DMA (50 μM)-supplemented medium and kept in the presence of this inhibitor, pH_i was 6.94 ± 0.1 ($n = 30$). This pH_i was significantly lower than that measured in control cells (7.35 ± 0.1; $n = 30$). As shown in Fig. 9*D*, the amount of releasable Ca^{2+} from the TG-sensitive store was about five times lower

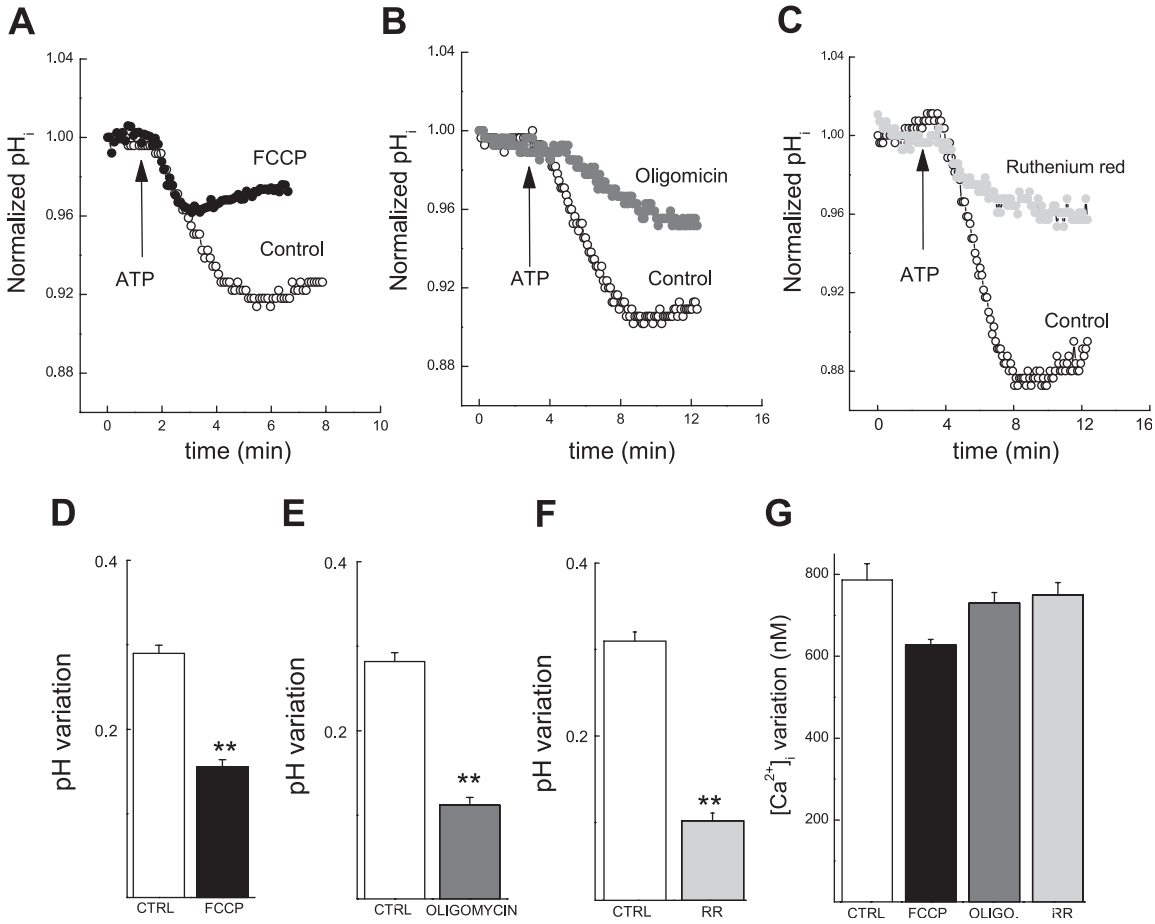

Fig. 6. Mitochondrial involvement in the intracellular acidification induced by ATP. *A*: typical traces showing the time course of change in pH_i after an application of 100 μM ATP in the absence (control, open circles) or in the presence of 5 μM FCCP (closed circles). Values are relative to basal pH_i, designated as 1. *B*: typical traces showing the time course of change in pH_i after an application of 100 μM ATP in the absence (control, open circles) or in the presence of 2 μM oligomycin (shaded circles). Values are relative to basal pH_i, designated as 1. *C*: typical traces showing the time course of change in pH_i after application of 100 μM ATP in the absence (control, open circles) or in the presence of 30 μM ruthenium red (shaded circles). Values are relative to basal pH_i, designated as 1. *D*: mean value of the change in the pH_i induced by 100 μM ATP alone (CTRL; $n = 64$) and in the presence of 5 μM FCCP ($n = 62$). *E*: mean values of the changes in the pH_i induced by 100 μM ATP alone (CTRL; $n = 60$) and in the presence of 2 μM oligomycin ($n = 60$). *F*: mean values of the change in the pH_i induced by 100 μM ATP alone (CTRL; $n = 45$) and in the presence of 30 μM ruthenium red (RR; $n = 44$). *G*: mean value of the change in $[Ca^{2+}]_i$ induced by 100 μM ATP under control condition (CTRL; $n = 49$), in the presence of 5 μM FCCP ($n = 30$), in the presence of 2 μM oligomycin ($n = 40$), and in the presence of ruthenium red (RR; $n = 32$). Bars represent changes in $[Ca^{2+}]_i$ expressed as means ± SE. $^{**}P < 0.01$, significantly different from control.

when pH_i was reduced (by the NH_4^+ pulse) than under control conditions (in which the pH_i was not modified). Indeed, the amplitude of the $[Ca^{2+}]_{cyt}$ elevation induced by TG (1 μM) in a Ca^{2+}-free medium was 103 ± 30 nM ($n = 33$), corresponding to 481 ± 148 nM ($n = 36$) in control cells. In the same manner (Fig. 9*E*), the maximal amount of Ca^{2+} released by ATP (100 μM) by the pH_i-lowering treatment reached 36 ± 16 nM ($n = 23$), corresponding to 15% of the release observed under control conditions (481 ± 148 nM; $n = 36$). Taken together, these results suggest that the decrease in the amount of releasable Ca^{2+} induced by ATP treatment, already described in this model (43), can result from the pH_i decrease generated by ATP. We thus investigated the effect of acidification on Ca^{2+} pool content, measured in Mag-fura-2 AM-loaded cells. The basal level of $[Ca^{2+}]_{ER}$ was directly assessed using the fluorescent Ca^{2+} indicator Mag-fura-2 AM. Imaging experiments with Mag-fura-2 AM were conducted on cells permeabilized by mild digitonin treatment. Figure 9*F* shows the time course of a typical experiment involving measurement of $[Ca^{2+}]_{ER}$ in DU-145 prostate cells in response to acidification of the intracellular buffer from 7.2 to 6.8 and to 6.4. Lowering pH of the intracellular buffer from 7.2 to 6.8 did not cause any modification of $[Ca^{2+}]_{ER}$. A pronounced decrease in pH from 7.2 to 6.4 triggered a rapid drop in $[Ca^{2+}]_{ER}$ followed by $[Ca^{2+}]_{ER}$ recovery due to Ca^{2+} reuptake into intracellular stores. This latter result suggests that the decrease in the pool of releasable Ca^{2+} under acidic conditions is not secondary to impairment of Ca^{2+} uptake by the endoplasmic reticulum in our experimental conditions.

We then tested whether pH_i decrease alone might be part of the mechanism that leads to ATP-induced growth arrest in DU-145 cells. To test this hypothesis, cells were treated for 48 h with DMA (50 μM) before pH_i and proliferation were assessed. As shown in Fig. 10*A*, 48-h treatment with DMA

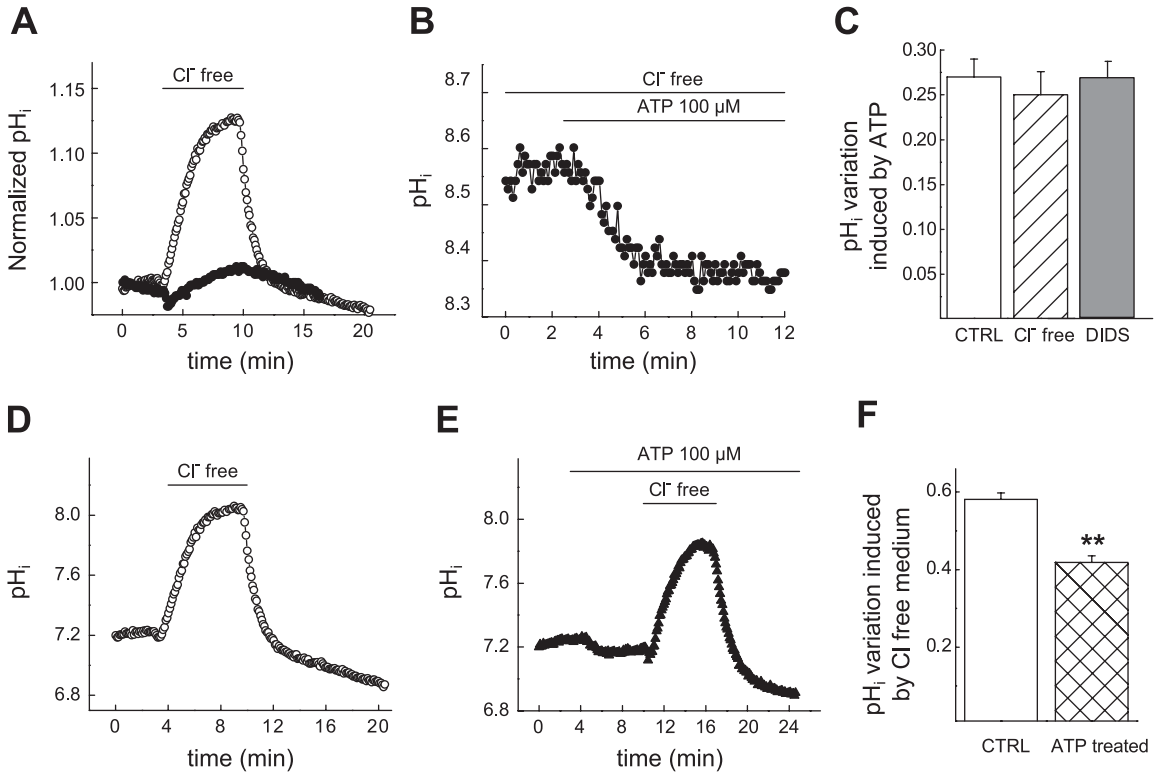

Fig. 7. Cl^-/HCO_3^- exchanger involvement in ATP-induced acidification. *A*: typical traces showing the time course of change in pH_i after an application of a Cl^--free medium in the absence (control, open circles) or in the presence of 100 μM 4,4′-diisothiocyanostilbene sulfonic acid (DIDS; closed circles). *B*: typical trace showing the time course of change in pH_i after application of 100 μM ATP in cells bathing in a Cl^--free medium. *C*: mean value of the change in pH_i induced by 100 μM ATP alone (CTRL; $n = 25$), in the absence of Cl^- ($n = 22$) and in the presence of 100 μM DIDS ($n = 23$). *D*: typical trace showing the time course of pH_i after application of a Cl^--free medium. *E*: typical trace showing the time course of pH_i after an application of a Cl^--free medium in the presence of 100 μM ATP. *F*: mean value of the change in the pH_i induced by a Cl^--free medium alone (CTRL; $n = 72$) and in the presence of 100 μM ATP (ATP treated; $n = 51$). Bars represent changes in $[Ca^{2+}]_i$ expressed as means ± SE. Results marked with ** $P < 0.01$, significantly different from control.

reduced the pH_i by the same order of magnitude as treatment with ATP (100 μM). pHi was 7.11 ± 0.1 ($n = 264$) and 7.10 ± 13 ($n = 225$), respectively, compared with the control value of 7.32 ± 0.08 ($n = 241$). A 48-h DMA treatment induced a reduction in cell growth. The cell growth was 59 ± 16% that of control (Fig. 10*B*). The growth rate inhibition induced by DMA cannot be explained by an increase in apoptosis, because no stimulation of apoptosis was observed in our experiments as determined using Hoechst staining (data not shown).We consequently thought it necessary to examine whether the pH decrease was the initial event leading to cell growth reduction. In these cells treated with DMA, the amount of releasable Ca^{2+} was reduced by 88% compared with control conditions (Fig. 10*C*). Indeed, $[Ca^{2+}]_i$ increase induced by TG (1 μM) was 36 ± 16 nM ($n = 23$) in cells treated for 48 h with DMA, whereas it was 295 ± 72 nM ($n = 19$) for cells cultured in control conditions. These results support the hypothesis that pH_i decrease may be the first element that leads to DU-145 cells growth reduction and suggests that the reduction in the amount of releasable Ca^{2+} induced by ATP (Fig. 10*C*) may be a consequence of pH_i decrease. Both the cell growth and the releasable Ca^{2+} reduction induced by DMA were more pronounced than those induced by ATP (Fig. 10, *B* and *E*). In effect, cell growth was 86 ± 5% of the control, and the decrease of releasable Ca^{2+} was ~34%. These results suggest that pH_i decrease is a part of the mechanism leading to the physiological ATP response.

DISCUSSION

In this study, we have demonstrated that exposure of human androgen-insensitive human prostate cancer DU-145 cells to ATP produces rapid, sustainable, and reversible intracellular acidification. Our data show that ATP-induced acidification results from an increase in $[Ca^{2+}]_i$. Our results also show that the specific effect on mitochondrial function accounts for the ATP- induced acidification of DU-145 cells. We therefore conclude that the F_0F_1-ATPase may participate in pH_i acidification induced by ATP.

Purinergic receptor involvement in ATP-induced acidification. The extracellular effects of nucleotides such as ATP are mediated by P_2 receptors. In DU-145 cells, it has been demonstrated that ATP induced an increase in $[Ca^{2+}]_i$ mediated by P_2 purinergic receptors (10). More recently, it was described that ATP-induced Ca^{2+} increase was linked to the PLC-IP_3 pathway (18, 43). Inhibition of this pathway with U-73122 inhibited the ATP-induced acidification in DU-145 cells. Furthermore, inhibition of P_2X receptors, which have been described to be activated by ATP in DU-145 cells (18), did not modify the intracellular acidification induced by ATP. We thus

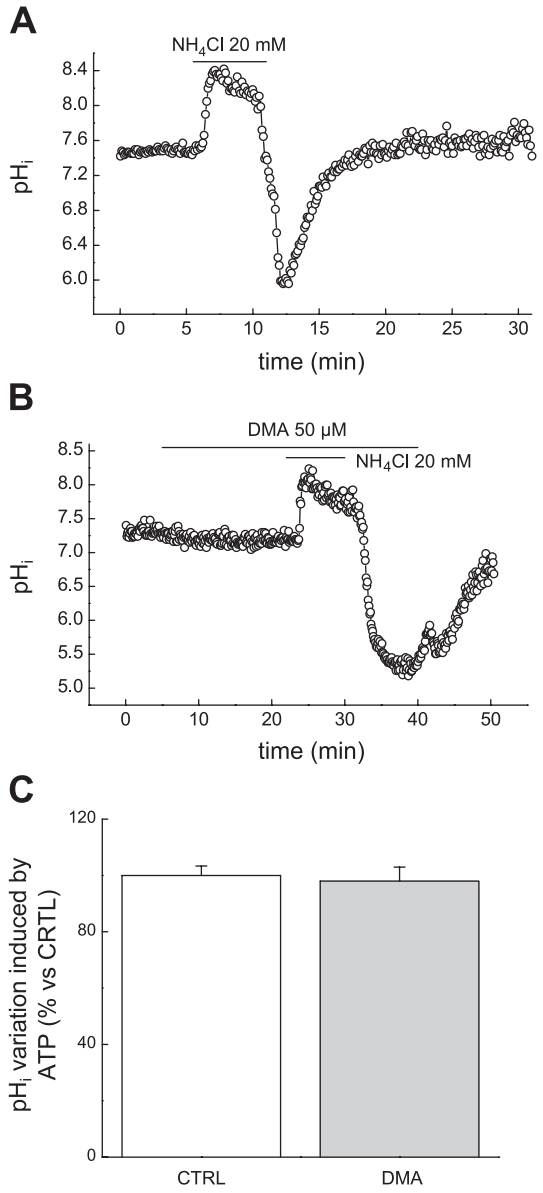

Fig. 8. Na^+/H^+exchanger involvement in ATP-induced acidification. *A*: typical trace showing the time course of pH_i after transient application of 20 mM NH_4Cl. *B*: typical trace showing the time course of pH_i after application of a NH_4Cl pulse in the presence of 50 μM dimethyl amiloride (DMA). *C*: mean value of the change in pH_i induced by 100 μM ATP alone (CTRL; $n = 25$) and in the presence of 50 μM DMA ($n = 13$). Values are relative to the change in the pH_i obtained with ATP designated as 100%. Bars represent change in pH_i and are expressed as means ± SE.

suggest that P_2 purinergic receptors are involved in the ATP signaling pathway, causing ATP to induce acidification in DU-145 cells.

Ca^{2+} involvement in ATP-induced acidification. Because it is well documented that ATP induces Ca^{2+} increase in DU-145 cells (18, 43), the link between intracellular Ca^{2+} increase and ATP-induced acidification was investigated. 2-APB, known to block Ca^{2+} entry in DU-145 cells (43), inhibits ATP-induced acidification, indicating that ATP-induced acidification results from an increase in $[Ca^{2+}]_i$. In addition, lowering extracellular Ca^{2+} or buffering $[Ca^{2+}]_i$ with EGTA-AM also inhibited ATP-induced acidification. Furthermore ATP-induced acidification could be mimicked by an artificial Ca^{2+} elevation induced by TG and ionomycin. Intracellular acidification was induced by Ca^{2+} influx and not by release from intracellular stores, because it was not observed after TG or ionomycin treatment in the absence of Ca^{2+} in the bath solution. Nevertheless, a small pH_i decrease was observed when ATP was applied in a Ca^{2+}-free medium. This result can be explained, first, by the different kinetics of Ca^{2+} release induced by ATP and TG. Indeed, we have demonstrated that metabotropic induced Ca^{2+} release is faster than TG- or ionomycin-induced Ca^{2+} release as shown in Fig. 9. Second, the decrease in the pH_i induced by ATP in a Ca^{2+}-free medium could result from an additional Ca^{2+}-independent mechanism.

NHE and Cl^-/HCO_3^- exchanger involvement in pH_i variation induced by ATP. ATP previously was described as inducing intracellular acidification in a large variety of models (19, 20, 25, 42). It has been reported that the exposure of human bronchial epithelial cells to ATP produced rapid, sustained, and reversible intracellular acidification (42). In human nasal epithelium, rat cardiomyocytes, bovine aortic endothelial cells, and osteoclasts, it was reported that external ATP produced a biphasic variation in pH_i. External ATP produced an initial acidification followed by realkalinization equal to or above the steady-state pH_i value (19, 20, 25). The differences in pH_i profiles observed in different cell lines may result from differences in the mechanisms by which ATP mediates its effect. In human bronchial epithelial cells (in which ATP induces a sustained intracellular acidification), it was suggested that acidification arises from the inhibition of NHE and from the activation of a proton conductance. In osteoclasts and cardiomyocytes (9, 29, 49), ATP also has been shown to induce transient acidification by transient activation of the Cl^-/HCO_3^- exchanger. At least four types of acid extrusion mechanisms—NHE, the Cl^-/HCO_3^- exchanger, the Na^+/HCO_3^- cotransporter, and the Na^+-dependent Cl^-/HCO_3^- exchanger—can be triggered during a pH_i decrease (48). The first is DMA sensitive, and the others are DIDS sensitive. We therefore tested whether ATP-induced acidification could result from an inhibition of NHE or from an activation of the Cl^-/HCO_3^- exchanger already described in other models. In our cells, the participation of NHE and Cl^-/HCO_3^- exchanger in ATP-induced acidification was ruled out. Indeed, NHE inhibition cannot participate in ATP-induced acidification in DU-145 cells, because blockage of NHE (which is functional in our model) by DMA did not reduce ATP-induced acidification. Furthermore, ATP-induced acidification was always observed in Cl^--free medium or in the presence of DIDS. This eliminated the possibility of activation of the Cl^-/HCO_3^- exchanger in the ATP-induced acidification in our model. Rather than being stimulated, the Cl^-/HCO_3^- exchanger activity was reduced during ATP exposure.

Cyclic nucleotide-induced acidification previously was reported to be dependent on $[Ca^{2+}]_i$ increase (20), because UTP was able to induce acidification in a Ca^{2+}-dependent manner in macrophages. In this model of UTP-induced, Ca^{2+}-dependent acidification, lipoxygenase metabolites were suggested as the acidification mediators. The involvement of this pathway in ATP-induced acidification in DU-145 cells remains to be determined.

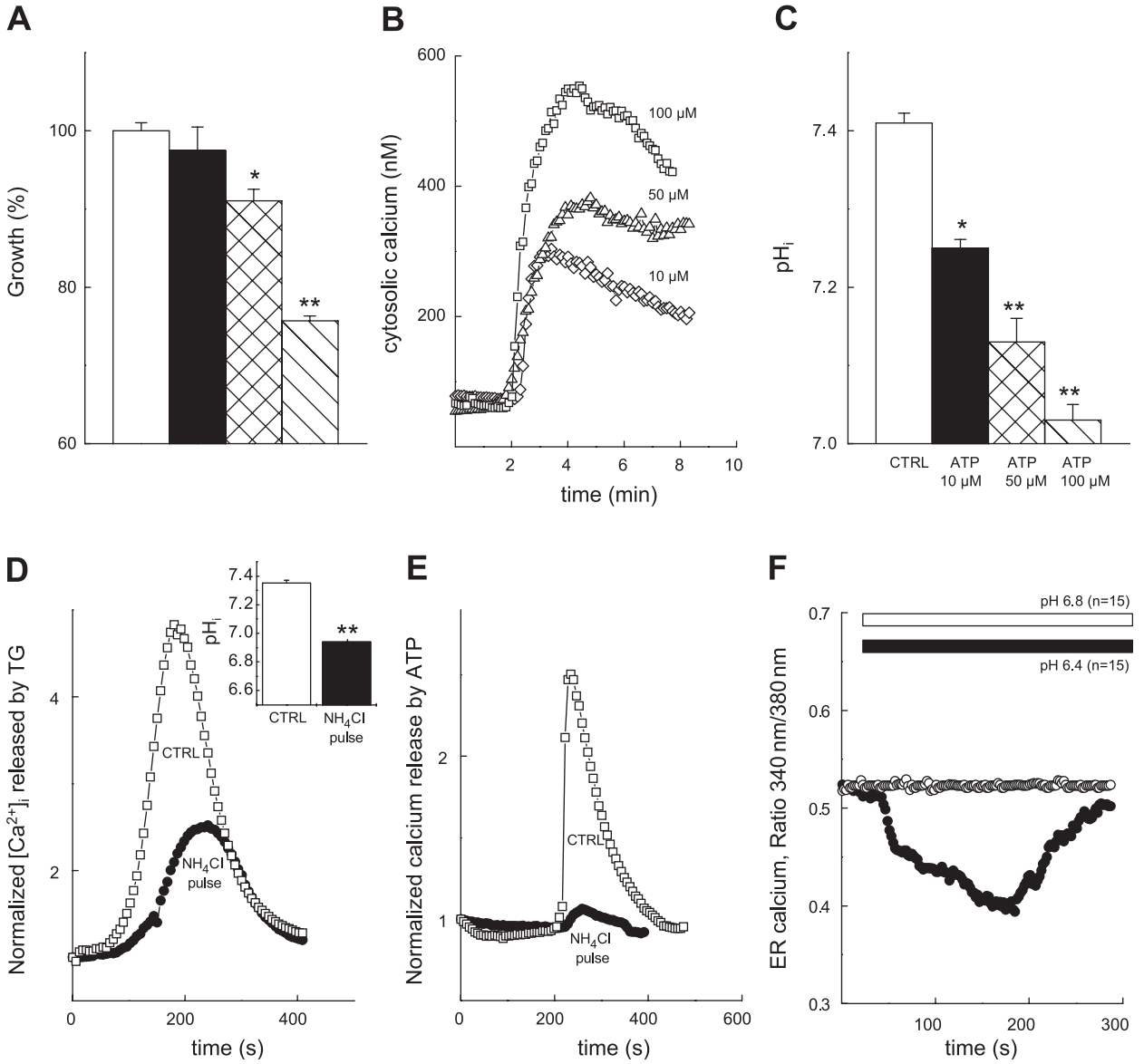

Fig. 9. Dose effect of extracellular ATP application on growth, $[Ca^{2+}]_i$, and pH_i after 2 days of treatment. *A*: action on DU-145 cell growth of extracellular ATP (10, 50, and 100 μM) after 2 days of treatment. *B*: action of extracellular ATP (10, 50, and 100 μM) on DU-145 $[Ca^{2+}]_i$. *C*: action of extracellular ATP (10, 50, and 100 μM) on DU-145 pH_i after 2 days of treatment. Intracellular acidification decreased the amount of $[Ca^{2+}]_i$ increase induced by TG and ATP. *D*: typical traces showing the time course of $[Ca^{2+}]_i$ after application of 1 μM TG in control conditions (CTRL, open squares) and on cells with low preliminary pH_i challenged with a NH_4Cl pulse in the presence of 50 μM DMA (closed circles). Values are relative to the basal $[Ca^{2+}]_i$, designated as 1. *Inset*: mean value of the pH_i under control conditions (CTRL; $n = 30$) and after a NH_4CL pulse performed in cells treated with 50 μM DMA ($n = 30$). *E*: typical traces showing the time course of $[Ca^{2+}]_i$ after application of 100 μM ATP in control conditions (open squares) and on cells with low pH_i previously challenged with a NH_4Cl pulse in the presence of 50 μM DMA (closed circles). Values are relative to the basal $[Ca^{2+}]_i$, designated as 1. *F*: measurement of $[Ca^{2+}]$ in the endoplasmic reticulum ($[Ca^{2+}]_{ER}$) presented as ratio of 340-nm/380-nm fluorescence in response to change in pH_i of the intracellular buffer from 7.2 to 6.8 (open circles) and from 7.2 to 6.4 (closed circles).

Mitochondrial involvement in the acidification induced by ATP. The effect of $[Ca^{2+}]_i$ increase on pH_i via the activation of glutamate receptors in neurons was previously described (15, 23). Furthermore, depolarization-induced acidification in vertebrate or invertebrate neurons also occurs through a Ca^{2+} influx (1, 40). More recently, the link between the Ca^{2+} influx and the depolarization-induced pH_i decrease has been described in dendrites (34, 36). A variety of mechanisms have been identified that might generate pH_i changes as a consequence of neuronal $[Ca^{2+}]_i$ increase: the passive binding of Ca^{2+} buffers in exchange for protons (17), plasma membrane Ca^{2+} extrusion (40), the stimulation of the metabolism (50), and mitochondrial Ca^{2+} uptake (45, 46). When $[Ca^{2+}]_i$ reaches the level at which the rate of Ca^{2+} influx into the mitochondria exceeds the rate of Ca^{2+} extrusion from the mitochondria, the mitochondria start to accumulate Ca^{2+}, which depolarizes the inner mitochondrial membrane. To compensate for the mitochondrial membrane potential drop, regulatory mechanisms

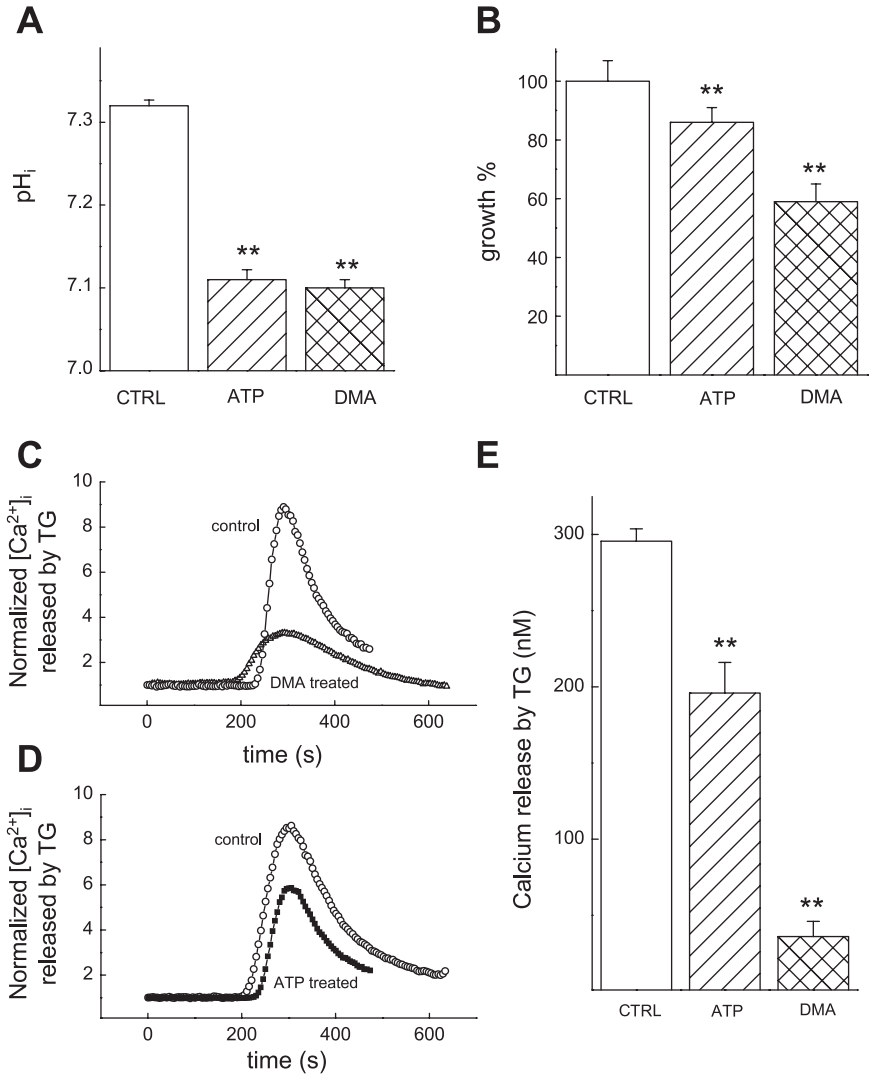

Fig. 10. *A*: pH_i measured after 2 days of treatment with 100 μM ATP or 50 μM DMA compared with pH_i of nontreated cells (CTRL). *B*: cell growth measured after 2 days of treatment with 100 μM ATP or 50 μM DMA compared with pH_i of nontreated cells (CTRL). *C*: typical traces showing the time course of $[Ca^{2+}]_i$ after an application of 1 μM TG in control conditions (open circle) and on cells treated for 2 days with 50 μM DMA (open triangles) Values are relative to the basal $[Ca^{2+}]_i$, designated as 1. *D*: typical traces showing the time course of $[Ca^{2+}]_i$ after an application of 1 μM TG in control conditions (control, open circles) and on cells treated for 2 days with 100 μM ATP (closed squares). Values are relative to the basal $[Ca^{2+}]_i$, designated as 1. *E*: mean values of the change in the $[Ca^{2+}]_i$ induced by 1 μM TG under control conditions (CTRL, $n = 19$) and in cells treated with 100 μM ATP (ATP, $n = 35$) or with 50 μM DMA (DMA, $n = 23$). Bars represent change in $[Ca^{2+}]_i$ expressed as means ± SE. Results marked with $^{**}P < 0.01$, significantly different from control.

that extrude extra protons from the mitochondrial matrix are activated. In our study using confocal imaging of rhod-2 fluorescence, we have demonstrated that ATP is able to induce Ca^{2+} influx in mitochondria. Furthermore, our results show that ATP induced a dissipation of the mitochondrial potential. This depolarization of mitochondria is transient, demonstrating the existence of a regulatory mechanism of the mitochondrial potential. These regulatory mechanisms, which compensate the mitochondrial membrane potential drop, extrude extra protons from the mitochondrial matrix. In our model, we have demonstrated that mitochondrial function accounts for a large part of the mechanism leading to ATP-induced acidification, because mitochondrial inhibitors reduce the effects of ATP on pH_i. Indeed, inhibition of the mitochondrial Ca^{2+} uniporter with ruthenium red reduced the ATP-induced acidification. In addition, we have shown that a reduction in the proton gradient across the inner mitochondrial membrane with rotenone and FCCP strongly reduced ATP-induced acidification, thereby indicating that a specific effect on mitochondrial function accounts for the ATP-induced acidification in DU-145 cells. Furthermore, inhibition of the F_0F_1-ATPase with oligomycin decreased ATP-induced acidification, suggesting that F_0F_1-ATPase may participate in pH_i acidification induced by ATP. Mitochondrial inhibitors block only 60% of the ATP-induced acidification, so we conclude that an additional mechanism that remains to be determined participates in ATP-induced acidification in DU-145 cells. Nevertheless, to our knowledge, this report is the first to clearly demonstrate the involvement of the mitochondrial function in Ca^{2+}-induced acidification in nonexcitable cells and ATP-induced acidification.

Involvement of pH_i in the Ca^{2+} release processes. Our results show that low pH_i downregulates the ability of Ca^{2+} to be released by ATP or by TG. Such a reduction in the Ca^{2+} release process was not due to a reduction in the $[Ca^{2+}]_{ER}$, because direct measurement of the $[Ca^{2+}]_{ER}$ as a function of pH_i did not show any modification of $[Ca^{2+}]_{ER}$ when pH_i fell to 6.8 and did show a transient decrease when pH_i dropped to 6.4. The downregulation of the Ca^{2+} release after the metabotropic stimulation observed at low pH_i is consistent with previously described results. In effect, the pH dependence of IP_3-induced Ca^{2+} release has been observed in smooth muscle cells, because intracellular alkalinization enhances the rate of IP_3-induced Ca^{2+} release (41). Similar results were obtained in human lymphocytes and pancreatic acinar cells (7, 38), and in

neurons the transient increase in $[Ca^{2+}]_i$ did not occur for pH_i below 7.1 (39). Furthermore, because alkalinization is able to increase the IP_3 level in chondrocytes (5), one might postulate that lowering pH_i could reduce the IP_3 production induced by ATP in our model. Investigators at our laboratory (43) recently demonstrated that the IP_3R1-to-IP_3R3 ratio in DU-145 cells was 8–92%. Moreover, IP_3R3 activity is strongly reduced by low pH_i compared with IP_3R1 (8). Thus the strong pH_i dependence of ATP-induced Ca^{2+} release observed in this study of DU-145 cells can be explained by considering the ratio between the different isoforms of the IP_3 receptors observed in our model as well as the strong pH dependence of IP_3R3.

Physiological involvement of ATP-induced acidification. Relatively small changes in pH_i can have a profound effect on a variety of cellular functions. For example, pH_i plays a role in the control of DNA synthesis, cellular proliferation, the rate of protein synthesis, cell fertilization, the regulation of cell volume, muscle contractibility, neurotransmitter reuptake, and apoptosis. Only a few studies have suggested the possible role of intracellular acidification in cancer cell lines. In the present study, we have shown that acidification by itself could be a part of the mechanism that leads to growth inhibition induced by ATP, because artificial acidification induced by DMA can reduce cell growth.

Our results show that pH_i decrease in DU-145 cells is dose-dependently linked to ATP concentration and is associated with a decrease in the Ca^{2+} store previously described in this model (43). We have demonstrated that artificial intracellular acidification can induce a decrease in Ca^{2+} release. In effect, in cells in which pH_i was reduced (by an NH_4^+ pulse in cells treated with DMA), Ca^{2+} release induced by TG or ATP also failed. Furthermore, TG-induced Ca^{2+} release was reduced in cells treated for 48 h with DMA alone, suggesting that pH_i decrease may be one of the mechanisms that leads to a decrease in $[Ca^{2+}]_i$ in DU-145 cells. Taken together, our results suggest that acidification is one of the major mechanisms leading to growth arrest induced by ATP and highlighting cross talk between pH_i and Ca^{2+} in prostate cancer cells.

REFERENCES

1. **Ahmed Z and Connor JA.** Intracellular pH changes induced by calcium influx during electrical activity in molluscan neurons. *J Gen Physiol* 75: 403–426, 1980.
2. **Alberts B, Bray D, Lewis J, Raff M, Roberts K, and Watson JD.** *Molecular Biology of the Cell* (3rd Ed.). New York: Garland Publishing, 1998.
3. **Alfonso A, Cabado AG, Vieytes MR, and Botana LM.** Calcium-pH crosstalks in rat mast cells: cytosolic alkalinization, but not intracellular calcium release, is a sufficient signal for degranulation. *Br J Pharmacol* 130: 1809–1816, 2000.
4. **Ballanyi K and Kaila K.** Activity-evoked changes in intracellular pH. In: *pH and Brain Function*, edited by Kaila K and Ransom BR. New York: Wiley-Liss, 1998, p. 291–308.
5. **Browning JA and Wilkins RJ.** The effect of intracellular alkalinisation on intracellular Ca^{2+} homeostasis in a human chondrocyte cell line. *Pflügers Arch* 444: 744–751, 2000.
6. **Budd SL and Nicholls DG.** A reevaluation of the role of mitochondria in neuronal Ca^{2+} homeostasis. *J Neurochem* 66: 403–411, 1996.
7. **Cabado AG, Alfonso A, Vieytes MR, Gonzalez M, Botana MA, and Botana LM.** Crosstalk between cytosolic pH and intracellular calcium in human lymphocytes: effect of 4-aminopyridin, ammoniun chloride and ionomycin. *Cell Signal* 12: 573–581, 2000.
8. **De Smet P, Parys JB, Vanlingen S, Bultynck G, Callewaert G, Galione A, De Smedt H, and Missiaen L.** The relative order of IP_3 sensitivity of types 1 and 3 IP_3 receptors is pH dependent. *Pflügers Arch* 438: 154–158, 1999.
9. **Desilets M, Pucéat M, and Vassort G.** Chloride dependence of pH modulation by β-adrenergic agonist in rat cardiomyocytes. *Circ Res* 75: 862–869, 1994.
10. **Fang WG, Pirnia F, Bang YJ, Myers CE, and Trepel JB.** P_2-purinergic agonists inhibit the growth of androgen-independent prostate carcinoma cells. *J Clin Invest* 89: 191–196, 1992.
11. **Feldman BJ and Feldman D.** The development of androgen-independent prostate cancer. *Nat Rev Cancer* 1:34–45, 2001.
12. **Friedberg I, Belzer I, Oged-Plesz O, and Kuebler D.** Activation of cell growth inhibitor by ectoprotein kinase-mediated phosphorylation in transformed mouse fibroblasts. *J Biol Chem* 270: 20560–20567, 1995.
13. **Gunter TE, Gunter KK, Sheu SS, and Gavin CE.** Mitochondrial calcium transport: physiological and pathological relevance. *Am J Physiol Cell Physiol* 267: C313–C339, 1994.
14. **Gunter TE and Pfeiffer DR.** Mechanisms by which mitochondria transport calcium. *Am J Physiol Cell Physiol* 258: C755–C786, 1990.
15. **Hartley Z and Dubinsky JM.** Changes in intracellular pH associated with glutamate excitotoxicity. *J Neurosci* 13: 4690–4699, 1993.
16. **Humez S, Collin T, Matifat F, Guilbault P, and Fournier F.** $InsP_3$-dependent Ca^{2+} oscillations linked to activation of voltage-dependent H^+ conductance in Rana esculenta oocytes. *Cell Signal* 8: 375–379, 1996.
17. **Irwin RP, Lin SZ, Long RT, and Paul SM.** *N*-methyl-D-aspartate induces a rapid, reversible, and calcium-dependent intracellular acidosis in cultured fetal rat hippocampal neurons. *J Neurosci* 14: 1352–1357, 1994.
18. **Janssens R and Boeynaems JM.** Effects of extracellular nucleotides and nucleosides on prostate carcinoma cells. *Br J Pharmacol* 132: 536–546, 2001.
19. **Kitazono T, Takeshige K, Cragoe EJ Jr, and Minakami S.** Involvement of calcium and protein kinase C in the activation of the Na^+/H^+ exchanger in cultured bovine aortic endothelial cells stimulated by extracellular ATP. *Biochim Biophys Acta* 1013: 152–158, 1989.
20. **Lin WW, Chang SH, and Wu ML.** Lipoxygenase metabolites as mediators of UTP-induced intracellular acidification in mouse RAW 264.7 macrophages. *Mol Pharmacol* 53: 313–321, 1998.
21. **Maaser K, Höpfner M, Kap H, Sutter AP, Barthel B, von Lampe B, Zeitz M, and Scherübl H.** Extracellular nucleotides inhibit growth of human oesophageal cancer cells via P_2Y_2-receptors. *Br J Cancer* 86: 636–644, 2002.
22. **McLean LA, Roscoe J, Jørgensen NK, Gorin FA, and Cala PM.** Malignant gliomas display altered pH regulation by NHE1 compared with nontransformed astrocytes. *Am J Physiol Cell Physiol* 278: C676–C688, 2000.
23. **Meech RW and Thomas RC.** Effect of measured calcium chloride injections on the membrane potential and internal pH of snail neurons. *J Physiol* 298: 111–129, 1980.
24. **Nicholls DG and Budd SL.** Mitochondria and neuronal survival. *Physiol Rev* 80: 315–360, 2000.
25. **Paradiso AM.** ATP-activated basolateral Na^+/H^+ exchange in human normal and cystic fibrosis airway epithelium. *Am J Physiol Lung Cell Mol Physiol* 273: L148–L158, 1997.
26. **Pouyssegur J, Franchi A, and Pages G.** pH_i, aerobic glycolysis and vascular endothelial growth factor in tumour growth. *Novartis Found Symp* 240: 186–198, 2001.
27. **Pozzan T, Rizzuto R, Volpe P, and Meldolesi J.** Molecular and cellular physiology of intracellular calcium stores. *Physiol Rev* 74: 595–636, 1994.
28. **Pucéat M, Clement O, and Vassort G.** Extracellular MgATP activates the Cl^-/HCO_3^- exchanger in single rat cardiac cells. *J Physiol* 444: 241–256, 1991.
29. **Pucéat M, Roche S, and Vassort G.** Src family tyrosine kinase regulates intracellular pH in cardiomyocytes. *J Cell Biol* 141: 1637–1646, 1998.
30. **Putney LK and Barber DL.** Na-H exchange-dependent increase in intracellular pH times G_2/M entry and transition. *J Biol Chem* 278: 44645–44649, 2003.
31. **Reshkin SJ, Bellizzi A, Caldeira S, Albarani V, Malanchi I, Poignee M, Alunni-Fabbroni M, Casavola V, and Tommasino M.** Na^+/H^+ exchanger-dependent intracellular alkalinization is an early event in malignant transformation and plays an essential role in the development of subsequent transformation-associated phenotypes. *FASEB J* 14: 2185–2197, 2000.
32. **Rich IN, Worthington-White D, Garden OA, and Musk P.** Apoptosis of leukemic cells accompanies reduction in intracellular pH after targeted inhibition of the Na^+/H^+ exchanger. *Blood* 95: 1427–1434, 2000.

33. **Rizzuto R, Bastianutto C, Brini M, Murgia M, and Pozzan T.** Mitochondrial Ca^{2+} homeostasis in intact cells. *J Cell Biol* 126: 1183–1194, 1994.
34. **Rizzuto R, Simpson AW, Brini M, and Pozzan T.** Rapid changes of mitochondrial Ca^{2+} revealed by specifically targeted recombinant aequorin. *Nature* 358: 325–327, 1992.
35. **Roos A and Boron WR.** Intracellular pH. *Physiol Rev* 51: 296–434, 1981.
36. **Schwiening CJ and Willoughby D.** Depolarization-induced pH microdomains and their relationship to calcium transients in isolated snail neurons. *J Physiol* 538: 371–382, 2002.
37. **Shrode LD, Tapper H, and Grinstein S.** Role of intracellular pH in proliferation, transformation, and apoptosis. *J Bioenerg Biomembr* 29: 393–399, 1997.
38. **Speake T and Elliott AC.** Modulation of calcium signals by intracellular pH in isolated pancreatic acinar cells. *J Physiol* 506: 415–430, 1998.
39. **Thomas RC.** The effects of HCl and $CaCl_2$ injections on intracellular calcium and pH in voltage-clamped snail (*Helix aspersa*) neurons. *J Gen Physiol* 120: 567–579, 2002.
40. **Trapp S, Lückermann M, Kaila K, and Ballanyi K.** Acidosis of hippocampal neurones mediated by a plasmalemmal Ca^{2+}/H^+ pump. *Neuroreport* 7: 2000–2004, 1996.
41. **Tsukioka M, Iino M, and Endo M.** pH dependence of inositol 1,4,5-trisphosphate-induced Ca^{2+} release in permeabilized smooth muscle cells of the guinea-pig. *J Physiol* 475: 369–375, 1994.
42. **Urbach V, Hélix N, Renaudon B, and Harvey BJ.** Cellular mechanisms for apical ATP effects on intracellular pH in human bronchial epithelium. *J Physiol* 543: 13–21, 2002.
43. **Vanoverberghe K, Mariot P, Vanden Abeele F, Delcourt P, Parys JB, and Prevarskaya N.** Mechanisms of ATP-induced calcium signaling and growth arrest in human prostate cancer cells. *Cell Calcium* 34: 75–85, 2003.
44. **Vereninov AA, Vassilieva IO, Yurinskaya VE, Matveev VV, Glushankova LN, Lang F, and Matskevitch JA.** Differential transcription of ion transporters, NHE1, ATP1B1, NKCC1 in human peripheral blood lymphocytes activated to proliferation. *Cell Physiol Biochem* 11: 19–26, 2001.
45. **Wang GJ, Randall RD, and Thayer SA.** Glutamate-induced intracellular acidification of cultured hippocampal neurons demonstrates altered energy metabolism resulting from Ca^{2+} loads. *J Neurophysiol* 72: 2563–2569, 1994.
46. **Werth JL and Thayer SA.** Mitochondria buffer physiological calcium loads in cultured rat dorsal root ganglion neurons. *J Neurosci* 14: 348–356, 1994.
47. **Willoughby D and Schwiening CJ.** Electrically evoked dendritic pH transients in rat cerebellar Purkinje cells. *J Physiol* 544: 487–499, 2002.
48. **Wu ML, Tsai ML, and Tseng YZ.** DIDS-sensitive pH_i regulation in single rat cardiac myocytes in nominally HCO_3^--free conditions. *Circ Res* 75: 123–132, 1994.
49. **Yu H and Ferrier J.** Osteoclast ATP receptor activation leads to a transient decrease in intracellular pH. *J Cell Sci* 108: 3051–3058, 1995.
50. **Zhan RZ, Fujiwara N, Tanaka E, and Shimoji K.** Intracellular acidification induced by membrane depolarization in rat hippocampal slices: roles of intracellular Ca^{2+} and glycolysis. *Brain Res* 780: 86–94, 1998.